CHAPTER 3

SYNTHESIS, SPECTROSCOPY AND BORONATION OF A NEW HETEROLEPTIC RUTHENIUM CYANIDE COMPLEX

Introduction

$[Ru(diimine)(CN)_4]^{2-}$ complexes

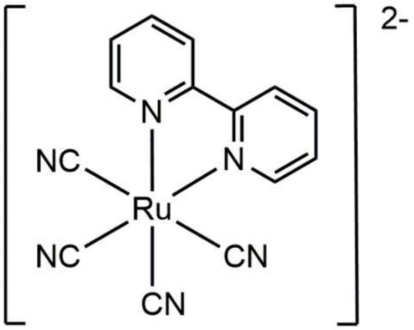

Figure 1: Structure of $[Ru(bpy)(CN)_4]^{2-}$.

Inspired by mounting evidence that the long-lived metal-to-ligand charge transfer (MLCT) excited state of $[Ru(bpy)_3]^{2+}$ featured an electron localized on just one bpy ligand, Scandola et al. first synthesized $[Ru(bpy)(CN)_4]^{2-}$ (Figure 1) in 1986 as a minimalistic model of Ru(II) diimine photosensitizers.[1] They observed that the luminescence and excited-state properties were very similar to $[Ru(bpy)_3]^{2+}$, but that the spectroscopic properties also featured strong solvatochromism. The magnitude of the solvatochromism is driven largely by specific solvent interactions with the cyanide ligands. In a systematic study of Ru-polypyridyl-cyanide complexes with 1-5 cyanides, Meyer et al. found that shifts in the C-N stretching frequency, MLCT absorption energy, and emission energy all correlated with the Gutmann acceptor number of the solvent and increased as a function of the number of cyanide ligands.[2]

These solvatochromic properties have driven much of the interest in $[Ru(bpy)(CN)_4]^{2-}$ and related $[Ru(diimine)(CN)_4]^{2-}$ complexes,[3–5] and several applications have been reported. PPN_2 $Ru(bpy)(CN)_4$ (PPN = bis(triphenylphosphine)iminium) can be used as a humidity sensor, as it reversibly turns from purple to yellow on exposure to water vapor.[6] Solvent-tunable dye sensitized solar cells have been produced using a carboxylate-modified bpy to append the molecule to TiO_2.[7]

The exposed lone pair on the cyanide nitrogen in $[Ru(diimine)(CN)_4]^{2-}$ complexes has also been exploited to form supramolecular assemblies through hydrogen bonding[8–13] or coordination to other metal centers.[14–21] These assemblies often have interesting luminescence or energy-transfer properties, and one such assembly has been exploited as a sensor and chemodosimeter for amines released during food spoilage.[15,16]

Borane Modification of Metal Cyanide Complexes

In 1963, Shriver observed that a number of cyanometallates could absorb an equivalent of borane per cyanide, resulting in a ca. 100 cm^{-1} shift in the C-N stretch to higher frequencies.[22] For the homoleptic cyanometallates, he found that the d-d transitions were unaffected by the coordination of borane, but the spectrum of $Fe(phen)_2(CN)_2$, which is dominated by MLCT transitions, blueshifted dramatically. This pair of observations indicates that formation of the borane adduct stabilizes metal-centered orbitals, but has no strong effect on the ligand-based orbitals. As a result, one expects that d-d transitions should remain relatively constant, MLCT transitions should blueshift, and ligand-to-metal charge transfer (LMCT) transitions should redshift on boronation; electrochemically, the same orbital shifts should produce anodic shifts in metal-centered redox processes while minimally affecting ligand-centered redox processes.

While this area of research had been fairly dormant since Shriver's work, it became of interest to the Gray group as a way of tuning the potential of cyanometallates in order to produce high-voltage redox flow battery electrolytes. As expected, McNicholas et al. found that addition of boranes to ferricyanide anodically shift the $Fe^{II/III}$ couple.[23] By examining cyclic voltammagrams containing substoichiometric BPh_3, which coordinates reversibly to the cyanides, they determined that there is a linear relationship between the number of boranes coordinated and the magnitude of the shift. Each equivalent of BPh_3 shifts the ferricyanide couple by ca. 260 mV, and for BCF, which coordinates irreversibly, a more dramatic 350 mV shift was observed. These observations were in line with previous publications which showed similar shifts in $Os^{II/III}$ [24] and $Re^{I/II}$ couples[25] on addition of the same boranes to cyanide ligands.

As of this writing, the study of boronation of homoleptic cyanometallates is very active within the Gray group, and manuscripts are now in preparation describing synthesis and spectroscopy of Co, Mn, Cr, Fe, Ru, Os, Ni, and Pt isocyanoborate complexes.[26–28]

Previous Work on Boronation of $[Ru(bpy)(CN)_4]^{2-}$ and related complexes

In an effort to develop symmetric redox flow battery electrolytes, the boronation of Fe(II) and Ru(II) cyanometallates containing bpy and phen has also been studied recently in the Gray group.[26,29] $[Ru(bpy)(CN)_4]^{2-}$, $[Fe(bpy)(CN)_4]^{2-}$, and $[Fe(phen)(CN)_4]^{2-}$ were each boronated with both BPh_3 and BCF. In each case, boronation produces a shift to higher frequency of the C-N stretches, a blueshift in the MLCT-dominated optical spectrum, and an anodic shift of the $M^{II/III}$ couple, with more dramatic shifts for BCF than BPh_3, reflecting its higher Lewis acidity. In the case of $[Ru(bpy)(CN)_4]^{2--}$, boronation also results in a luminescent excited state that is two orders of magnitude longer-lived, although the BPh_3 adduct undergoes photodecomposition with loss of the borane.

Although a redox flow battery has not yet been successfully created from it, this research resulted in the synthesis of $[Ru(bpy)(CN\text{-}BCF)_4]^{2--}$, which in MeCN has two reversible redox events separated by more than 3.5 V. This voltage would greatly improve upon the working voltages of existing flow battery systems. The following work represents an effort to improve the reductive stability of this molecule.

Results & Discussion

Synthesis and Spectroscopy of $[Ru(^{CF3}bpy)(CN)_4]^{2-}$

$K_2Ru(^{CF3}bpy)(CN)_4$ (^{CF3}bpy = 4,4'-bis(trifluoromethyl)-2,2'-bipyridine) was synthesized analogously to other $K_2Ru(diimine)(CN)_4$ complexes[30] and converted to the PPN salt by precipitation from aqueous solution. $PPN_2Ru(^{CF3}bpy)(CN)_4$ is received initially as a brick-red solid which is soluble in polar organic solvents and turns dark green when fully dehydrated. The complex was characterized by ^1H and ^{19}F NMR spectroscopy, solid-state IR spectroscopy, elemental analysis, and X-ray crystallography.

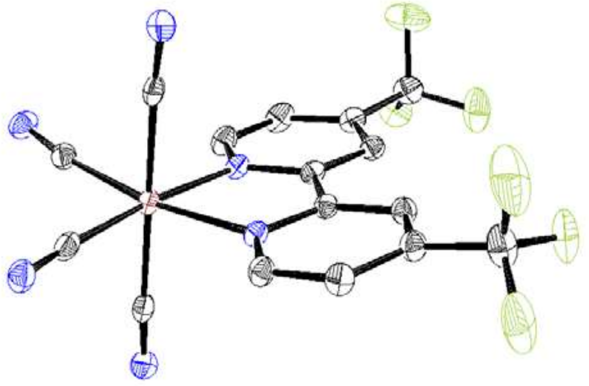

Figure 2: Molecular structure of $PPN_2Ru(^{CF3}bpy)(CN)_4$. Thermal ellipsoids set at 50% probability. Cations, hydrogen atoms, and solvent molecules omitted for clarity.

The X-ray crystallographic data (Figure 2) reveals a negligible difference in metal-ligand contacts between $[Ru(^{CF3}bpy)(CN)_4]^{2-}$ and the parent bpy complex,[6] which suggests that there is minimal difference in backbonding, despite the more electron-deficient bipyridine ligand. The C-N stretches detected in the solid state by FT-IR spectroscopy (Figure 3) support this interpretation. Typical complexes in this family have three closely-spaced strong peaks between 2030-2060 cm^{-1} and a weaker peak around 2090 cm^{-1}; the closely-spaced peaks were not resolved, but the observed peaks at 2062 and 2090 cm^{-1} are in line with related complexes.

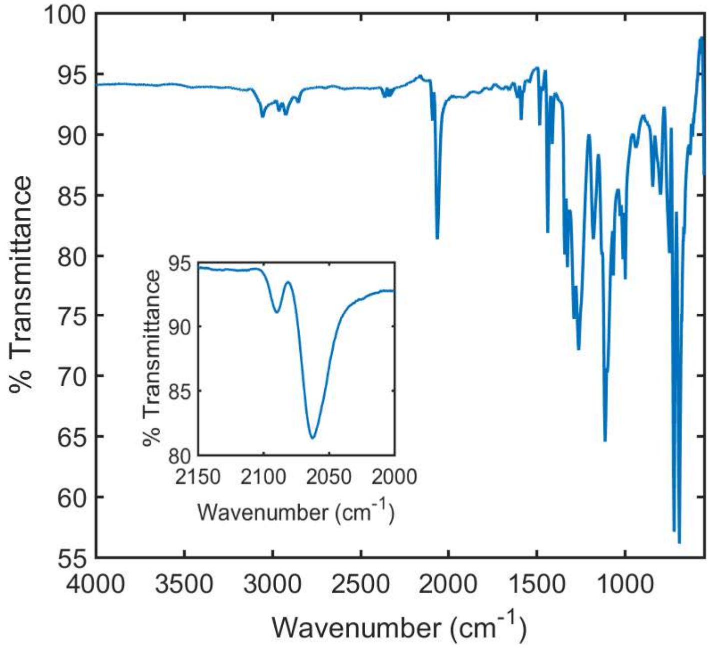

Figure 3: IR spectrum of $PPN_2Ru(^{CF3}bpy)(CN)_4$ with C-N stretches highlighted in inset.

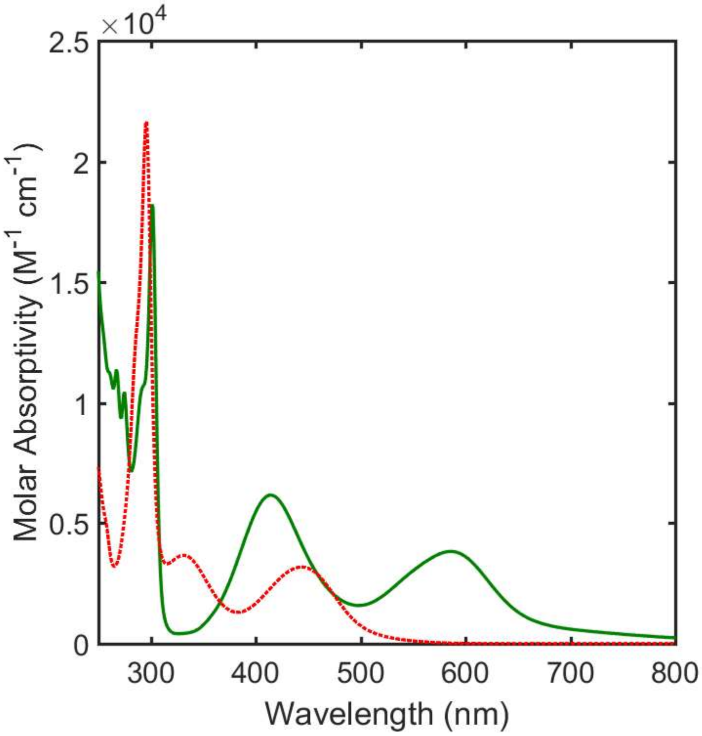

Figure 4: UV-Vis spectra of $[Ru(^{CF3}bpy)(CN)_4]^{2-}$ in water (red broken trace, K salt) and acetonitrile (green solid trace, PPN salt).

$[Ru(diimine)(CN)_4]^{2-}$ complexes are well-known for their solvatochromism, which results both from having a ground-state dipole which interacts with polar solvents and the ability to accept hydrogen bonds at the N-termini of the cyanide ligands.[5] Likewise, $[Ru(^{CF3}bpy)(CN)_4]^{2-}$ displays strong solvatochromism, with the lowest-energy MLCT transition redshifting ca. 5500 cm^{-1} when the solvent is changed from water to acetonitrile (Figure 4). In water, the spectrum displays three distinct bands, which can be assigned as two MLCT transitions and a ^{CF3}bpy-based π-π* transition based on their extinction coefficients (~10^3 $M^{-1}cm^{-1}$ for MLCT transitions and ~10^4 for π-π*). Both MLCT transitions are dramatically shifted by the change in solvent, but the π-π* transition shifts only slightly (ca. 550 cm^{-1}), indicating that cyanide lone pair interactions are able to shift the d(Ru) orbitals while minimally affecting the

^{CF3}bpy orbitals. The absorption bands are also redshifted relative to most other [Ru(diimine)(CN)$_4$]$^{2-}$ complexes (Table 1), reflecting the low-lying π orbitals of ^{CF3}bpy relative to bpy and other commonly-used diimines. In this respect, ^{CF3}bpy displays similar electronic properties to bpz, but without the exposed lone pairs which hydrogen bond with water.

Table 1: Comparison of room temperature photophysical data for [Ru(^{CF3}bpy)(CN)$_4$]$^{2-}$ and selected [Ru(diimine)(CN)$_4$]$^{2-}$ complexes. ^{R}bpy indicates R in the 4,4' positions of bipyridine.

Diimine ligand	Solvent	λ_{max} (nm)(ε (M^{-1} cm^{-1}))	λ_{em} (nm) (τ (ns))	Reference
bpy	H_2O	400	610(101)	1
	H_2O	404(4100)	624(100)	11
	MeCN	535	790(7)	8
^{Me}bpy	H_2O	392	600(115)	31
	MeCN	530	780(7)	31
bpym	D_2O	437(2200)	(3.4)	19
	MeCN	575	(0.25)	19
bpz	H_2O	465(5700)	704(5)	32
	MeCN	554		32
^{HOOC}bpy	MeCN	515	750	7
^{CF3}bpy	H_2O	443(3170)	706	This work
	MeCN	589(3770)	N.O. below 930	This work

While [Ru(diimine)(CN)$_4$]$^{2-}$ displays weak luminescence in aqueous solution (Figure S6), no luminescence was observed in the solid state or 2-MeTHF solution at room temperature or 77 K, suggesting that the emission in the dehydrated form may be redshifted beyond the 930 nm detection limit of the instruments used.

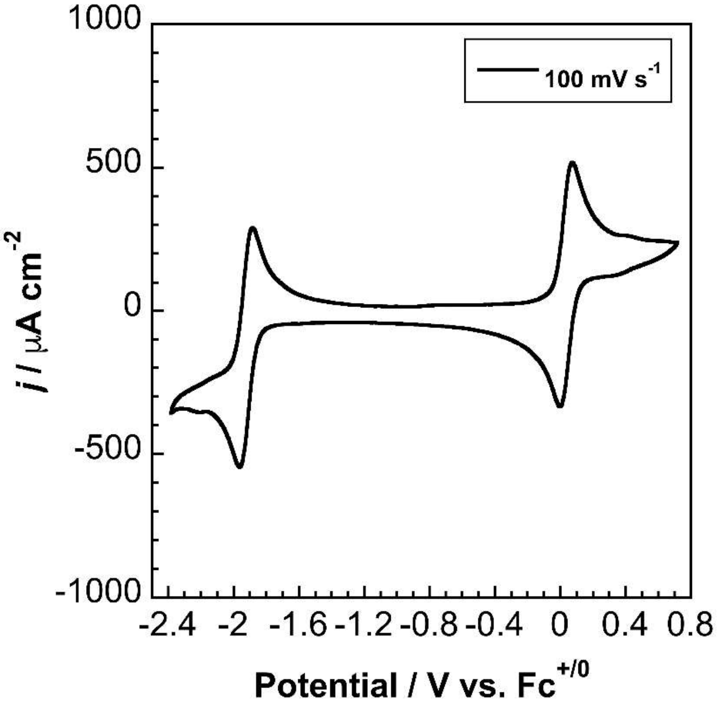

Figure 5: Cyclic voltammagram of 33 mM PPN_2 $Ru(^{CF3}bpy)(CN)_4$ in 0.2 M Bu_4NPF_6-supported acetonitrile. Working electrode: glassy carbon. Counter electrode: Pt wire.

The cyclic voltammagram of PPN_2 $Ru(^{CF3}bpy)(CN)_4$ in 0.2 M Bu_4NPF_6-supported acetonitrile displays two redox events at 0.05 and -1.92 V vs. $Fc^{+/0}$ corresponding to oxidation of the metal center to Ru(III) and reduction of the ^{CF3}bpy ligand, respectively (Figure 5). The peak current ratios for both waves are close to unity and the peak-to-peak separations are ca. 79 mV and independent of scan rate, indicating diffusion-controlled reversible electron transfer. While the parent bpy complex features a second irreversible reduction presumed to be deligation of bpy^{2-},[33] no such reduction or decomposition is observed for $[Ru(^{CF3}bpy)(CN)_4]^{2-}$. The reductive stability of ^{CF3}bpy in this system is accompanied by a 330 mV anodic shift in the $bpy^{0/-}$ couple relative to the parent complex and a 230 mV anodic shift in the $Ru^{2+/3+}$

couple. These shifts indicate that not only is ^{CF3}bpy more easily reduced than bpy, but that inductive effects result in a harder to oxidize Ru center.

Boronation with BCF and Spectroscopy

The tris(pentafluorophenyl)borane (BCF) adduct PPN_2 Ru(^{CF3}bpy)(CN-BCF)$_4$ was prepared in inert atmosphere by mixing DCM solutions of PPN_2 Ru(^{CF3}bpy)(CN)$_4$ and BCF and heating. On addition of the colorless BCF solution, the dark green PPN_2 Ru(^{CF3}bpy)(CN)$_4$ solution rapidly turns yellow. The resulting complex is an air-stable, luminescent yellow solid which is extremely soluble in polar organic solvents and has been characterized by ^{1}H, ^{19}F, and ^{11}B NMR spectroscopy, solid state IR spectroscopy, elemental analysis, and X-ray crystallography.

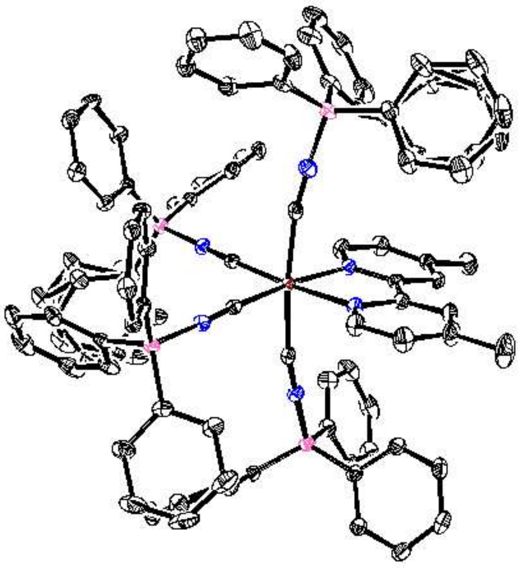

Figure 6: Molecular structure of PPN_2 Ru(^{CF3}bpy)(CN-BCF)$_4$. Thermal ellipsoids set at 50% probability. Cations, hydrogen and fluorine atoms, and solvent molecules omitted for clarity.

On addition of the borane, there is negligible change in the C-N distances and only a small shortening (ca. 0.05 Å) of the Ru-C distances (Figure 6). This observation is in line with the trends observed on addition of BCF to ferricyanide,[23] and likely results from a balancing of the bond-lengthening effect of N-donation to the borane and the bond-shortening effect of increased backbonding from Ru to the more π-acidic isocyanoborate. Crystallization of the related heteroleptic borane adducts has been stymied by their high solubility,[26,29] so more direct comparisons are not currently possible. Presumably due to steric crowding, the axial isocyanoborate ligands bow significantly (Ru-C-N bond angle 170°) over the plane of the bipyridine ligand, while those in the plane of the bipyridine remain close to linear. However, the crystal structure of PPN[Fe(phen)(CN-BPh$_3$)$_4$] does not display the same bowing effect (Ru-C-N = 176°), so there may be an electronic or crystal packing effect at play.

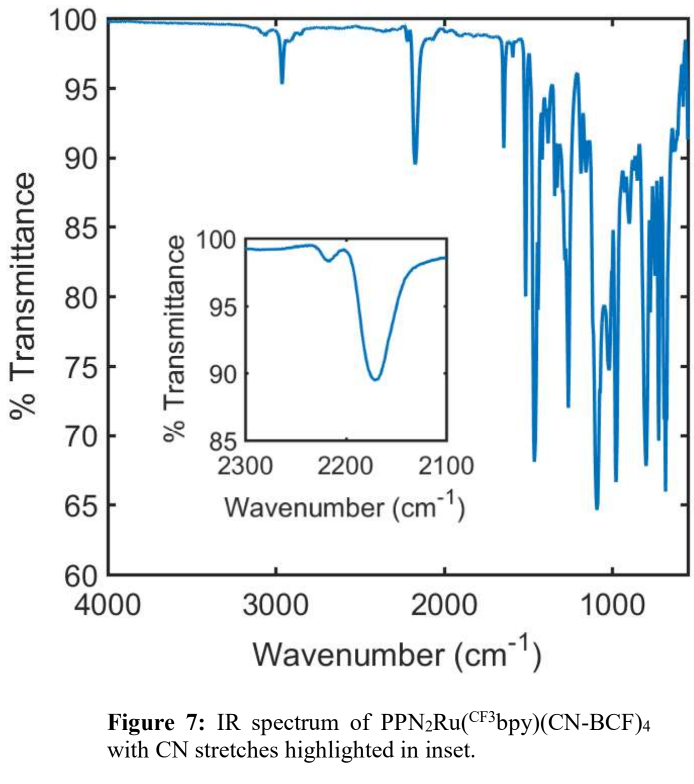

Figure 7: IR spectrum of PPN$_2$Ru(^{CF3}bpy)(CN-BCF)$_4$ with CN stretches highlighted in inset.

The C-N stretches in $[Ru(^{CF3}bpy)(CN\text{-}BCF)_4]^{2-}$ are shifted to much higher frequency (> 100 cm^{-1}, Figure 7). This observation, which indicates that the C-N bond is strengthened by coordination of the borane, is also in line with the shifts observed in ferricyanide[23] and other heteroleptic Ru complexes.[26,29]

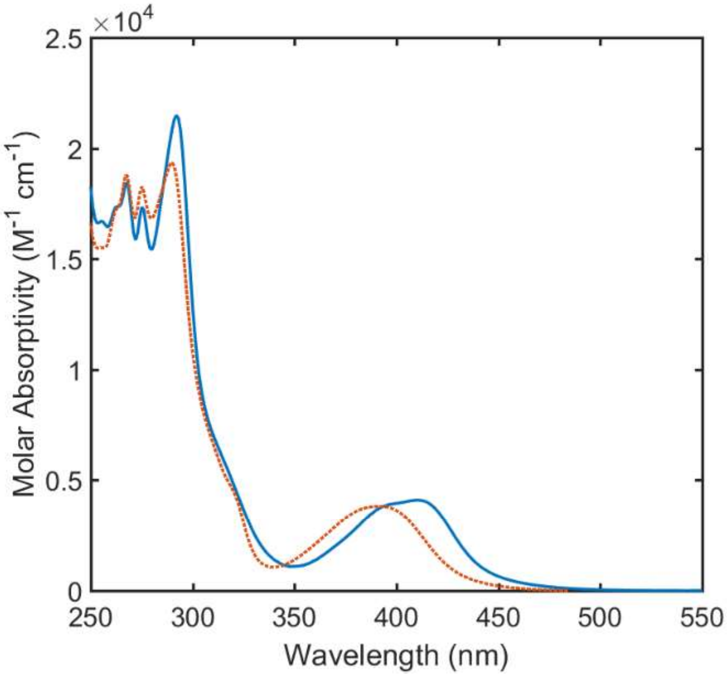

Figure 8: UV-Vis spectra for $PPN_2Ru(^{CF3}bpy)(CN\text{-}BCF)_4$ in DCM (blue solid trace) and MeCN (orange broken trace).

Addition of the boranes to $[Ru(^{CF3}bpy)(CN)_4]^{2-}$ induces a large blueshift in the optical absorption maximum, as the stronger Lewis acidity of BCF relative to water induces the cyanide ligands to become much better π acceptors. This strong ligand field lowers the energy of the Ru-d(π) orbitals, while minimally affecting the ^{CF3}bpy π orbitals, resulting in a blueshift in MeCN of the lowest-energy MLCT by nearly 8500 cm^{-1}. The boronated complex displays solvatochromism (Figure 8), with a slightly redshifted and split MLCT in DCM, indicating there is still a dipole in the ground state. $[Ru(^{CF3}bpy)(CN\text{-}BCF)_4]^{2-}$ is also brightly emissive at 545 nm, with a long excited-state lifetime of 3.4 μs and high quantum yield of 14.4%, and is photostable for weeks in solution under room lights.

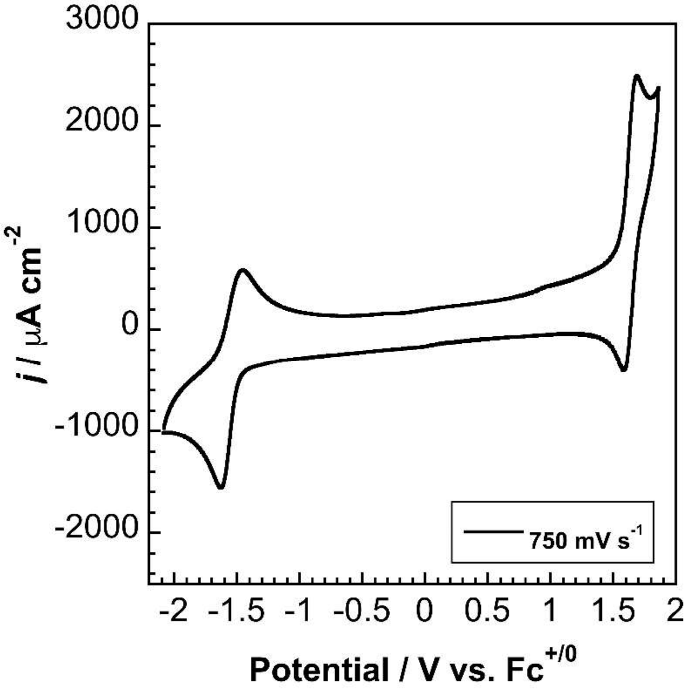

Figure 9: Cyclic voltammagram of 2.3 mM PPN$_2$ Ru(^{CF3}bpy)(CN-BCF)$_4$ in 0.2 M Bu$_4$NPF$_6$-supported acetonitrile. Working electrode: glassy carbon. Counter electrode: Pt wire.

Electrochemically, boronation with BCF induces a large anodic shift of 1.58 V in the potential of the Ru$^{2+/3+}$ couple along with a 390 mV anodic shift of the ^{CF3}bpy$^{0/.-}$ couple (Figure 9), comparable to the shifts observed for the parent bpy complex.[26,29] While the peak current ratio for the ^{CF3}bpy$^{0/.-}$ remains near-unity, the peak-to-peak separation increases with increasing scan rate, indicating that the electron transfer is reversible but slow on the timescale of the scan rates used. The heterogeneous charge-transfer rate constant (k_0) determined by Nicholson analysis (see Figure S5) of the appropriate variable scan rate data is 0.009 cm s^{-1}. The peak current ratios for the

$Ru^{2+/3+}$ couple deviate significantly from unity (average for all scan rates measured = 0.79) and decreases as the scan rate decreases, indicating a loss of reversibility attributable to an EC mechanism. Because the $Ru^{2+/3+}$ couple occurs very near the edge of the stability window for Bu_4NPF_6-supported MeCN, it is impossible to determine whether this electrochemical irreversibility is inherent to PPN_2 $Ru(^{CF3}bpy)(CN\text{-}BCF)_4$ or a result of solvent or supporting electrolyte decomposition.

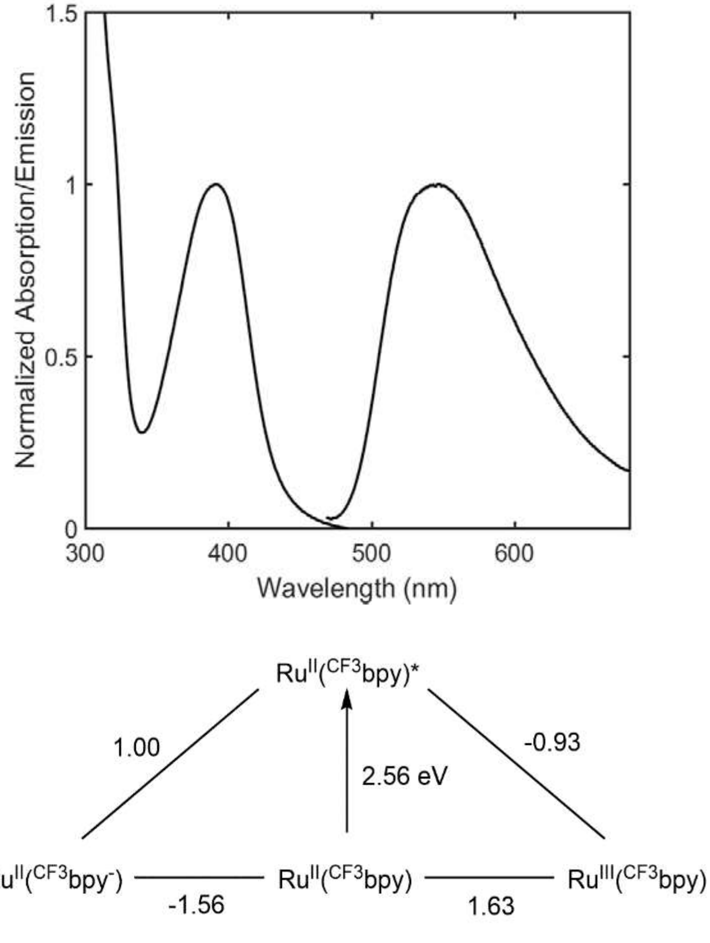

Figure 10: Top: room temperature absorption and emission data for $[Ru(^{CF3}bpy)(CN\text{-}BCF)_4]^{2-}$ in acetonitrile. Bottom: Modified Latimer diagram with potentials given in V vs. $Fc^{+/0}$.

Combining the electrochemical and photophysical data, a modified Latimer diagram can be constructed (Figure 10) to estimate the excited-state redox potentials for $[Ru(^{CF3}bpy)(CN\text{-}BCF)_4]^{2-}$. $[Ru(^{CF3}bpy)(CN\text{-}BCF)_4]^{2-}$ is expected to be a strong excited-state oxidant and modest excited state reductant, with an excited state oxidation potential comparable to $[Ru(bpz)_3]^{2+}$.[34]

Conclusion

A new member of the $[Ru(diimine)(CN)_4]^{2-}$ has been synthesized using the ^{CF3}bpy ligand, and it displays spectroscopic properties expected for an electron-withdrawing diimine. Notably, the library of $[Ru(diimine)(CN)_4]^{2-}$ complexes with electron-withdrawing diimine ligands is currently limited to bis(diazines) and ^{HOOC}bpy. $[Ru(^{CF3}bpy)(CN)_4]^{2-}$ represents an addition to this library that is nonreactive to protons, which may be desirable for certain applications.

The borane adduct $[Ru(^{CF3}bpy)(CN\text{-}BCF)_4]^{2-}$ has also been synthesized, and it represents an important step toward high voltage symmetric redox flow battery electrolytes with a voltage difference of 3.2 V. While the $Ru^{2+/3+}$ couple occurs too close to the edge of the solvent stability window to be useful as a flow battery electrolyte, the enhanced stability of the $^{CF3}bpy^{0/-}$ couple indicates that a different isocyanoborato complex of ^{CF3}bpy such as $Ru(^{CF3}bpy)_2(CN\text{-}BCF)_2$ might be able to achieve the right balance of properties.

$[Ru(^{CF3}bpy)(CN\text{-}BCF)_4]^{2-}$ also has luminescence properties that suggest it may be a useful photoredox catalyst. With 1 V of oxidizing power vs. $Fc^{+/0}$, it may be a competent catalyst for photooxidations that currently utilize $[Ru(bpz)_3]^{2+}$ or $[Ir[dF(CF_3)ppy]_2(dtbbpy)]^+$ as catalysts.

References

(1) Bignozzi, C. A.; Chiorboli, C.; Indelli, M. T.; Rampi Scandola, M. A.; Varani, G.; Scandola, F. Simple Poly(Pyridine)Ruthenium(II) Photosensitizer: (2,2'-Bipyridine)Tetracyanoruthenate(II). *J. Am. Chem. Soc.* **1986**, *108* (24), 7872–7873. https://doi.org/10.1021/ja00284a084.

(2) Timpson, C. J.; Bignozzi, C. A.; Sullivan, B. P.; Kober, E. M.; Meyer, T. J. Influence of Solvent on the Spectroscopic Properties of Cyano Complexes of Ruthenium(II). *J. Phys. Chem.* **1996**, *100* (8), 2915–2925. https://doi.org/10.1021/jp953179m.

(3) Shen, C.; Yu, F.; Chu, W.-K.; Xiang, J.; Tan, P.; Luo, Y.; Feng, H.; Guo, Z.-Q.; Leung, C.-F.; Lau, T.-C. Synthesis, Structures and Photophysical Properties of Luminescent Cyanoruthenate(II) Complexes with Hydroxylated Bipyridine and Phenanthroline Ligands. *RSC Adv.* **2016**, *6* (90), 87389–87399. https://doi.org/10.1039/C6RA16319J.

(4) Herrera, J.-M.; Pope, S. J. A.; Meijer, A. J. H. M.; Easun, T. L.; Adams, H.; Alsindi, W. Z.; Sun, X.-Z.; George, M. W.; Faulkner, S.; Ward, M. D. Photophysical and Structural Properties of Cyanoruthenate Complexes of Hexaazatriphenylene. *J. Am. Chem. Soc.* **2007**, *129* (37), 11491–11504. https://doi.org/10.1021/ja072672w.

(5) Ward, M. D. [Ru(Bipy)(CN)4]2− and Its Derivatives: Photophysical Properties and Its Use in Photoactive Supramolecular Assemblies. *Coord. Chem. Rev.* **2006**, *250* (23), 3128–3141. https://doi.org/10.1016/j.ccr.2006.02.012.

(6) Evju, J. K.; Mann, K. R. Synthesis and Spectroscopic Investigations of a Crystalline Humidity Sensor: Bis(Triphenylphosphine)Iminium 2,2'-Bipyridyltetracyanoruthenate. *Chem. Mater.* **1999**, *11* (6), 1425–1433. https://doi.org/10.1021/cm980323i.

(7) Argazzi, R.; Bignozzi, C. A.; Yang, M.; Hasselmann, G. M.; Meyer, G. J. Solvatochromic Dye Sensitized Nanocrystalline Solar Cells. *Nano Lett.* **2002**, *2* (6), 625–628. https://doi.org/10.1021/nl0255395.

(8) Rampi, M. A.; Indelli, M. T.; Scandola, F.; Pina, F.; Parola, A. J. Photophysics of Supercomplexes. Adduct between Ru(Bpy)(CN)42- and the [32]Ane-N8H88+ Polyaza Macrocycle. *Inorg. Chem.* **1996**, *35* (11), 3355–3361. https://doi.org/10.1021/ic951590i.

(9) Borsarelli, C. D.; Braslavsky, S. E.; Indelli, M. T.; Scandola, F. Photophysics of Supercomplexes. A Laser-Induced Optoacoustic Study of the Adducts between Ru(Bpy)(CN)42− and Polyaza Macrocycles. *Chem. Phys. Lett.* **2000**, *317* (1), 53–58. https://doi.org/10.1016/S0009-2614(99)01360-3.

(10) Pina, F.; Parola, A. J. Photochemistry of Supramolecular Species Involving Anionic Coordination Compounds and Polyammonium Macrocyclic Receptors. *Coord. Chem. Rev.* **1999**, *185–186*, 149–165. https://doi.org/10.1016/S0010-8545(98)00265-3.

(11) Simpson, N. R. M.; Ward, M. D.; Morales, A. F.; Barigelletti, F. Solvatochromism as a Mechanism for Controlling Intercomponent Photoinduced Processes in a Bichromophoric Complex Containing [Ru(Bpy)3]2+ and [Ru(Bpy)(CN)4]2− Units. *J. Chem. Soc. Dalton Trans.* **2002**, No. 12, 2449–2454. https://doi.org/10.1039/B201597H.

(12) Loiseau, F.; Marzanni, G.; Quici, S.; Indelli, M. T.; Campagna, S. An Artificial Antenna Complex Containing Four Ru(Bpy)32+-Type Chromophores as Light-Harvesting Components and a Ru(Bpy)(CN)42− Subunit as the Energy Trap. A Structural Motif Which Resembles the Natural Photosynthetic Systems. *Chem. Commun.* **2003**, No. 2, 286–287. https://doi.org/10.1039/B211122E.

(13) Bergamini, G.; Saudan, C.; Ceroni, P.; Maestri, M.; Balzani, V.; Gorka, M.; Lee, S.-K.; van Heyst, J.; Vögtle, F. Proton-Driven Self-Assembled Systems Based on Cyclam-Cored Dendrimers and [Ru(Bpy)(CN)4]2-. *J. Am. Chem. Soc.* **2004**, *126* (50), 16466–16471. https://doi.org/10.1021/ja0450814.

(14) Derossi, S.; Baca, S. G.; Miller, T. A.; Adams, H.; Jeffery, J. C.; Ward, M. D. Formation and Structural Chemistry of the Unusual Cyanide-Bridged Dinuclear Species [Ru2(NN)2(CN)7]3− (NN=2,2'-Bipyridine or 1,10-Phenanthroline). *Inorganica Chim. Acta* **2009**, *362* (4), 1282–1288. https://doi.org/10.1016/j.ica.2008.06.017.

(15) Chow, C.-F.; Lam, M. H. W.; Wong, W.-Y. Design and Synthesis of Heterobimetallic Ru(II)–Ln(III) Complexes as Chemodosimetric Ensembles for the Detection of Biogenic Amine Odorants. *Anal. Chem.* **2013**, *85* (17), 8246–8253. https://doi.org/10.1021/ac401513j.

(16) Chow, C.-F.; Kong, H.-K.; Leung, S.-W.; Chiu, B. K. W.; Koo, C.-K.; Lei, E. N. Y.; Lam, M. H. W.; Wong, W.-T.; Wong, W.-Y. Heterobimetallic Ru(II)−Eu(III) Complex as Chemodosimeter for Selective Biogenic Amine Odorants Detection in Fish Sample. *Anal. Chem.* **2011**, *83* (1), 289–296. https://doi.org/10.1021/ac102393f.

(17) Lazarides, T.; Easun, T. L.; Veyne-Marti, C.; Alsindi, W. Z.; George, M. W.; Deppermann, N.; Hunter, C. A.; Adams, H.; Ward, M. D. Structural and Photophysical Properties of Adducts of [Ru(Bipy)(CN)4]2- with Different Metal Cations: Metallochromism and Its Use in Switching Photoinduced Energy Transfer. *J. Am. Chem. Soc.* **2007**, *129* (13), 4014–4027. https://doi.org/10.1021/ja068436n.

(18) Baca, S. G.; Adams, H.; Sykes, D.; Faulkner, S.; Ward, M. D. Three-Component Coordination Networks Based on [Ru(Phen)(CN)4]2− Anions, near-Infrared Luminescent Lanthanide(III) Cations, and Ancillary Oligopyridine Ligands: Structures and Photophysical Properties. *Dalton Trans.* **2007**, No. 23, 2419–2430. https://doi.org/10.1039/B702235B.

(19) Adams, H.; Alsindi, W. Z.; Davies, G. M.; Duriska, M. B.; Easun, T. L.; Fenton, H. E.; Herrera, J.-M.; George, M. W.; Ronayne, K. L.; Sun, X.-Z.; et al. New Members of the [Ru(Diimine)(CN)4]2− Family: Structural, Electrochemical and Photophysical Properties. *Dalton Trans.* **2006**, *0* (1), 39–50. https://doi.org/10.1039/B509042C.

(20) Davies, G. M.; Pope, S. J. A.; Adams, H.; Faulkner, S.; Ward, M. D. Structural and Photophysical Properties of Coordination Networks Combining [Ru(Bipy)(CN)4]2- Anions and Lanthanide(III) Cations: Rates of Photoinduced Ru-to-Lanthanide Energy Transfer and Sensitized Near-Infrared Luminescence. *Inorg. Chem.* **2005**, *44* (13), 4656–4665. https://doi.org/10.1021/ic050512k.

(21) Hidalgo-Luangdilok, Carmela.; Bocarsly, A. B.; Woods, R. E. Electrochemically-Modulated Photoluminescence at the Chemically Derivatized Electrode: [CdRu(CN)4 (Bipyridine)]0/+ Modified Electrodes. *J. Phys. Chem.* **1990**, *94* (5), 1918–1924. https://doi.org/10.1021/j100368a037.

(22) Shriver, D. F. Preparation and Structures of Metal Cyanide-Lewis Acid Bridge Compounds. *J. Am. Chem. Soc.* **1963**, *85* (10), 1405–1408. https://doi.org/10.1021/ja00893a011.

(23) J. McNicholas, B.; H. Grubbs, R.; R. Winkler, J.; B. Gray, H.; Despagnet-Ayoub, E. Tuning the Formal Potential of Ferrocyanide over a 2.1 V Range. *Chem. Sci.* **2019**, *10* (12), 3623–3626. https://doi.org/10.1039/C8SC04972F.

(24) Chu, W.-K.; Yiu, S.-M.; Ko, C.-C. Neutral Luminescent Bis(Bipyridyl) Osmium(II) Complexes with Improved Phosphorescent Properties. *Organometallics* **2014**, *33* (23), 6771–6777. https://doi.org/10.1021/om500630c.

(25) Chu, W.-K.; Ko, C.-C.; Chan, K.-C.; Yiu, S.-M.; Wong, F.-L.; Lee, C.-S.; Roy, V. A. L. A Simple Design for Strongly Emissive Sky-Blue Phosphorescent Neutral Rhenium Complexes: Synthesis, Photophysics, and Electroluminescent Devices. *Chem. Mater.* **2014**, *26* (8), 2544–2550. https://doi.org/10.1021/cm4038654.

(26) Ngo, D. X.; Grubbs, R. H.; Gray, H. B.; McNicholas, B. J. Electronic Structures and Photophysics of [M(Diimine)(CN-BR3)4]2- (M = Fe, Ru) Complexes. **Manuscript in Preparation**.

(27) McNicholas, B.; Winkler, J. R.; Gray, H. B. Electronic Structure of Boronated, Group VIII Hexacyanometalates and Their Utility in Non-Aqueous Redox Flow Batteries and Cold Climate Energy Storage. **Manuscript in preparation**.

(28) Nie, C.; McNicholas, B. J.; Gray, H. B.; Grubbs, R. H. **Manuscript In Preparation**.

(29) Ngo, D. X. High Voltage Fe(II) and Ru(II) Symmetric Redox Flow Battery Electrolytes. Senior Thesis, California Institute of Technology, Pasadena, CA, 2019.

(30) Jiwan, J. L. H.; Wegewijs, B.; Indelli, M. T.; Scandola, F.; Braslavsky, S. E. Volume Changes Associated with Intramolecular Electron Transfer during MLCT State Formation. Time-Resolved Optoacoustic Studies of Ruthenium Cyano Complexes. *Recl. Trav. Chim. Pays-Bas-J. R. Neth. Chem. Soc.* **1995**, *114* (11–12), 542-.

(31) Indelli, M. T.; Ghirotti, M.; Prodi, A.; Chiorboli, C.; Scandola, F.; McClenaghan, N. D.; Puntoriero, F.; Campagna, S. Solvent Switching of Intramolecular Energy Transfer in Bichromophoric Systems: Photophysics of (2,2‘-Bipyridine)Tetracyanoruthenate(II)/Pyrenyl Complexes. *Inorg. Chem.* **2003**, *42* (18), 5489–5497. https://doi.org/10.1021/ic034185x.

(32) Garcia Posse, M. E.; Katz, N. E.; Baraldo, L. M.; Polonuer, D. D.; Colombano, C. G.; Olabe, J. A. Comparative Bonding and Photophysical Properties of 2,2’-Bipyridine and 2,2’-Bipyrazine in Tetracyano Complexes Containing Ruthenium and Osmium. *Inorg. Chem.* **1995**, *34* (7), 1830–1835. https://doi.org/10.1021/ic00111a034.

(33) Roffia, S.; Ciano, M. Electrochemical Behaviour of Dicyanobis(2,2'-Bipyridine) Ruthenium(II) and Dicyanobis(1,10-Phenanthroline) Ruthenium(II) Complexes. *J. Electroanal. Chem. Interfacial Electrochem.* **1977**, *77* (3), 349–359. https://doi.org/10.1016/S0022-0728(77)80280-5.

(34) Prier, C. K.; Rankic, D. A.; MacMillan, D. W. C. Visible Light Photoredox Catalysis with Transition Metal Complexes: Applications in Organic Synthesis. *Chem. Rev.* **2013**, *113* (7), 5322–5363. https://doi.org/10.1021/cr300503r.

(35) Krause, R. A.; Violette, C. An Improved Synthesis of Potassium Hexacyanoruthenate(II). *Inorganica Chim. Acta* **1986**, *113* (2), 161–162. https://doi.org/10.1016/S0020-1693(00)82239-2.

(36) Bard, A. J.; Faulkner, L. R. *Electrochemical Methods: Fundamentals and Applications*, 2nd ed.; John Wiley & Sons: Hoboken, NJ, 2001.

(37) Nicholson, R. S. Theory and Application of Cyclic Voltammetry for Measurement of Electrode Reaction Kinetics. *Anal. Chem.* **1965**, *37* (11), 1351–1355. https://doi.org/10.1021/ac60230a016.

(38) Lavagnini, I.; Antiochia, R.; Magno, F. An Extended Method for the Practical Evaluation of the Standard Rate Constant from Cyclic Voltammetric Data. *Electroanalysis* **2004**, *16* (6), 505–506. https://doi.org/10.1002/elan.200302851.

(39) Sattler, W.; Ener, M. E.; Blakemore, J. D.; Rachford, A. A.; LaBeaume, P. J.; Thackeray, J. W.; Cameron, J. F.; Winkler, J. R.; Gray, H. B. Generation of Powerful Tungsten Reductants by Visible Light Excitation. *J. Am. Chem. Soc.* **2013**, *135* (29), 10614–10617. https://doi.org/10.1021/ja4047119.

(40) Suzuki, K.; Kobayashi, A.; Kaneko, S.; Takehira, K.; Yoshihara, T.; Ishida, H.; Shiina, Y.; Oishi, S.; Tobita, S. Reevaluation of Absolute Luminescence Quantum Yields of Standard Solutions Using a Spectrometer with an Integrating Sphere and a Back-Thinned CCD Detector. *Phys. Chem. Chem. Phys.* **2009**, *11* (42), 9850–9860. https://doi.org/10.1039/B912178A.

(41) Crosby, G. A.; Demas, J. N. Measurement of Photoluminescence Quantum Yields. Review. *J. Phys. Chem.* **1971**, *75* (8), 991–1024. https://doi.org/10.1021/j100678a001.

Methods

General Considerations

Potassium hexacyanoruthenate(II) was synthesized by a known procedure[35]. 4,4'-trifluoromethyl-2,2'-bipyridine (^{CF3}bpy, Strem), bis(triphenylphosphine)iminium chloride (PPNCl, Millipore Sigma), and tris(pentafluorophenyl)borane (BCF, TCI) were used as received. NMR spectra were collected on a Varian 400 MHz spectrometer (δ in ppm, m: multiplet, s: singlet, d: doublet, t: triplet). UV-visible spectra were collected on a Cary 50 Bio or Cary 500 spectrometer. Solid-state infrared spectra were collected on a Thermo Scientific Nicolet iS5 FT-IR spectrometer with an iD5 ATR diamond.

Synthesis & Characterization

$PPN_2Ru(^{CF3}bpy)(CN)_4$

$K_2Ru(^{CF3}bpy)(CN)_4$ was synthesized with a modified version of the procedure published by Jiwan.[30] To a boiling solution of $K_4Ru(CN)_6$ (400 mg, .908 mmol) and ^{CF3}bpy (305 mg, 1.04 mmol) in 50 mL 1:1 methanol:water was added 400 µL 3.6 N H_2SO_4 (pH 4). The solution was refluxed for 24 h, over which time it slowly turned red, then cooled to room temperature and neutralized. Excess ^{CF3}bpy was removed by filtration and the solvent was removed. The remaining residue was purified by gel-filtration chromatography on a Sephadex G-15 column. Elution with water gave a main orange band free of excess $K_4Ru(CN)_6$. The main fraction was dried under vacuum to give $K_2Ru(^{CF3}bpy)(CN)_4$, yield 30%. The cation was exchanged by precipitation from concentrated aqueous solution with a saturated solution of PPNCl (307 mg, .535 mmol in 20 mL water). The resulting brick-red precipitate was collected by filtration and dried in a desiccator or under vacuum until it turned green, yield 326 mg (25%). Single crystals suitable for X-ray diffraction analysis were grown by slow evaporation from DCM solution. ^{1}H NMR (400 MHz, CD_2Cl_2): δ

10.02 (d, J = 8 Hz, 2H, 6,6’-H), 8.12 (s, 2H, 3,3’-H), 7.69-7.65 (m, 24H, PPN), 7.52-7.44 (m, 36H, PPN), 7.40 (d, J = 8 Hz, 2H, 5,5’-H). ^{19}F NMR (CD_2Cl_2): δ -64.71. IR (cm^{-1}, CN stretches) 2062, 2090. Anal. Calcd for $C_{88}H_{66}F_6N_8P_4Ru$: C, 67.13; H, 4.23; N, 7.12. Found: C, 64.21; H, 4.28; N, 5.55.

$PPN_2Ru(^{CF3}bpy)(CN\text{-}BCF)_4$

In a nitrogen-filled glovebox, $PPN_2Ru(^{CF3}bpy)(CN)_4$ (100 mg, 0.0637 mmol) and excess BCF (133 mg, 0.261 mmol) were each dissolved in minimal DCM. The two solutions were combined, causing a rapid color change from green to red to yellow. The solution was stirred for 1 h, then dried under vacuum. The resulting luminescent yellow solid was washed 3 x 10 mL hexanes, then dried thoroughly under vacuum. The resulting air-stable material was then further purified by flash chromatography on silica gel (eluent gradient from 100% hexanes to 90% dichloromethane in hexanes), affording 131 mg yellow product (0.0362 mmol, 56% yield). Single crystals suitable for X-ray diffraction analysis were grown from a saturated ethanol solution at –25°C. ^{1}H NMR (400 MHz, CD_2Cl_2): δ 9.22 (d, J = 4 Hz, 2H, 6,6’-H), 8.29 (s, 2H, 3,3’-H), 7.65-7.59 (m, 14H, PPN + 5,5’-H), 7.51-7.40 (m, 48H, PPN). ^{19}F NMR (CD_2Cl_2): δ -65.48 (s, 6F, CF_3), -134.54 (dd, 12F, *o*-F), -135.00 (dd, 12F, *o*-F), -161.57 (t, 6F, *p*-F), -162.03 (t, 6F, *p*-F), -167.01 (td, 12F, *m*-F), -167.29 (td, 12F, *m*-F). ^{11}B NMR (CD_2Cl_2): δ -14.09. IR (cm^{-1}, CN stretches) 2171, 2216. Anal. Calcd for $C_{160}H_{66}F_{66}N_8P_4Ru$: C, 53.05; H, 1.84; N, 3.09. Found: C, 51.69; H, 2.09; N, 2.76.

Electrochemical Measurements

Cyclic voltammagrams were taken in a nitrogen-filled glovebox with a Gamry Reference 600 potentiostat in a standard 3-electrode cell containing a 3 mm diameter glassy carbon working electrode, a 0.01 M $Ag^{+/0}$ in 0.1 M $TBAPF_6$/MeCN quasireference electrode, and a platinum wire counter electrode and compensated for 85% of the measured uncompensated resistance (R_u) value.

Diffusion coefficients were calculated from linear fits of plots of the peak current versus the square root of the scan rate using the Randles-Sevcik equation (Equation S1),[36] where i_p (A) is the peak current, n is the number of electrons transferred (1), F (C mol^{-1}) is the Faraday constant, C (mol cm^{-1}) is the bulk concentration of analyte, ν (V s^{-1}) is the scan rate, D_O (cm^2 s^{-1}) is the diffusion coefficient of the oxidized analyte, R (J mol^{-1} K^{-1}) is the ideal gas constant, and T (K) is the temperature.

$$i_p = 0.446nFAC\left(\frac{nF\nu D_O}{RT}\right)^{1/2} \quad (S1)$$

The heterogeneous electron transfer rate constant (k_0) for the ^{CF3}bpy$^{0/\cdot-}$ couple of PPN$_2$Ru(^{CF3}bpy)(CN -BCF)$_4$ was determined using Nicholson's kinetic parameter Ψ[37] along with Lavagnini's numerical interpretation of Ψ[38] (Equations S2 and S3).

$$\Psi = k_0\left(\frac{\pi D n\nu F}{RT}\right)^{-1/2} \quad (S2)$$

$$\Psi = \frac{-.06288 + .0021\chi}{1 - 0.017\chi} \quad (S3)$$

χ (mV) is the peak-to-peak separation. For sufficiently fast scan rates with respect to the electron transfer (i.e. in the region where χ is observed to vary with scan rate, where Ψ becomes small), plots of Ψ vs. $\nu^{-1/2}$ become linear, and k_0 may be calculated from the slope. For the other electrochemical couples observed, χ did not vary with the scan rates used, and would have required very high (> 3 V/s) scan rates for this analysis.

Photophysical Measurements

Steady-state and time-resolved spectroscopic measurements were carried out in the Beckman Institute Laser Resource Center (California Institute of Technology) using methods described previously.[39]

Quantum yields (φ_{PL}) were measured by comparison of deaerated, optically dilute solutions of the molecule of interest to $[Ru(bpy)_3](PF_6)_2$ in aerated and deaerated MeCN ($\varphi_{PL} = 0.018$ for aerated solutions and 0.095 for aerated solutions[40]) according to Equation S4.[41]

$$\varphi = \varphi_{ref} \frac{A_{ref}}{A} \frac{I}{I_{ref}} \frac{\eta^2}{\eta_{ref}{}^2} \quad \text{(S4)}$$

Subscript "ref" refers to the reference solutions, A are the absorbances at the exciting wavelength (450 nm for all measurements), I are the integrated emission intensities, and η are the refractive indices of the solvents used. Absorption measurements were taken before and after emission spectra to ensure there was no photodecomposition. Emission spectra were taken twice with different integration times to ensure there were no significant differences.

The resulting luminescence decay traces were fitted as an exponential decay to determine the excited state lifetimes (τ).

Supporting Data

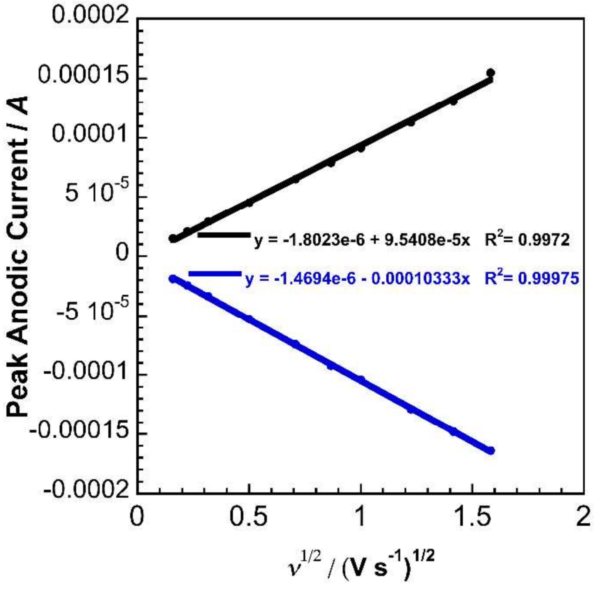

Figure S1: Randles-Sevcik plot for $PPN_2Ru(^{CF3}bpy)(CN)_4$; D = 5.7 x 10^{-6} cm^2 s^{-1}.

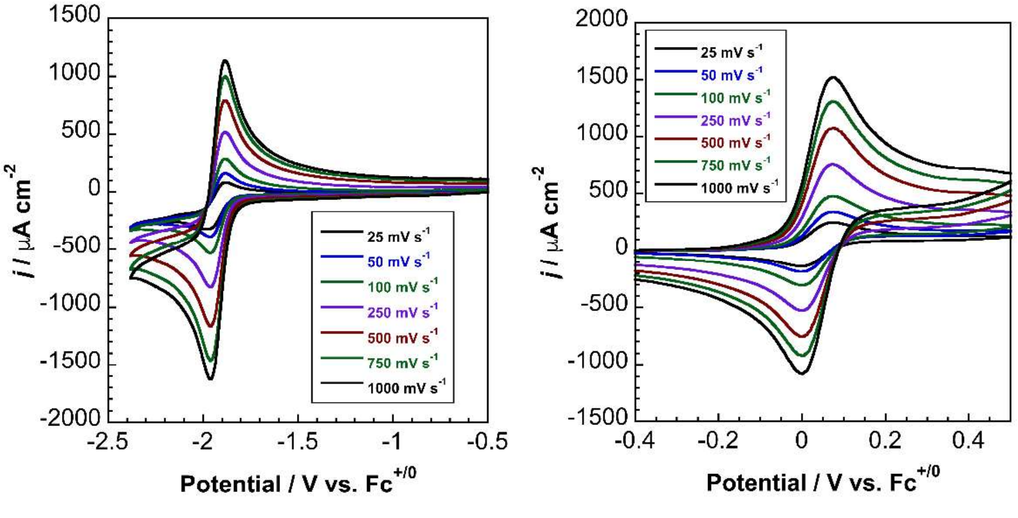

Figure S2: Variable scan rate cyclic voltammagrams for $PPN_2Ru(^{CF3}bpy)(CN)_4$. 33 mM PPN_2 $Ru(^{CF3}bpy)(CN)_4$ in 0.2 M Bu_4NPF_6-supported acetonitrile. Working electrode: glassy carbon. Counter electrode: Pt wire.

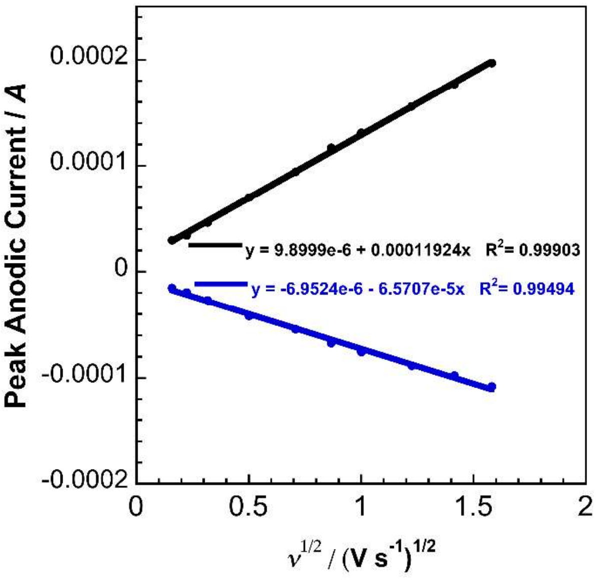

Figure S3: Randles-Sevcik plot for PPN$_2$Ru(^{CF3}bpy)(CN-BCF)$_4$; D = 7.4 x 10^{-6} cm^2 s^{-1} (top), 2.4 x 10^{-6} cm^2 s^{-1} (bottom).

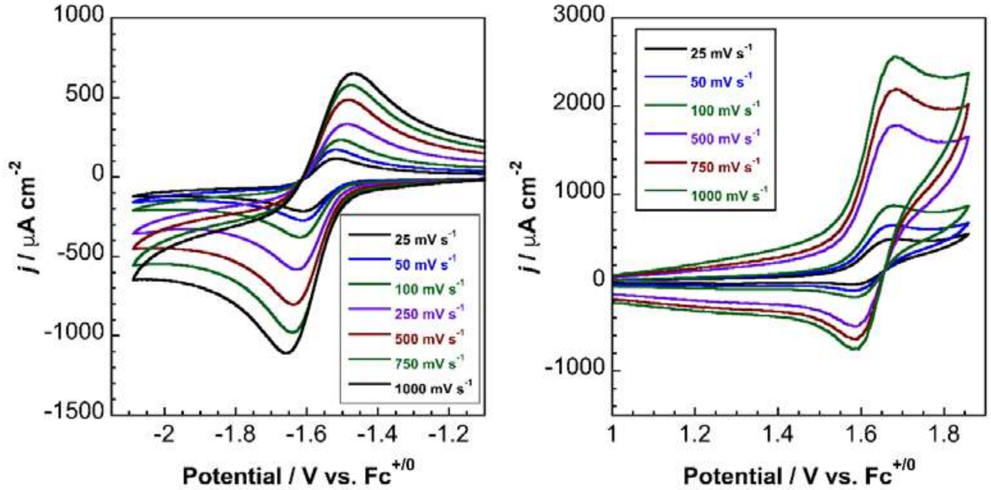

Figure S4: Variable scan rate cyclic voltammetry of PPN$_2$Ru(^{CF3}bpy)(CN-BCF)$_4$. . 2.3 mM PPN$_2$ Ru(^{CF3}bpy)(CN-BCF)$_4$ in 0.2 M Bu$_4$NPF$_6$-supported acetonitrile. Working electrode: glassy carbon. Counter electrode: Pt wire.

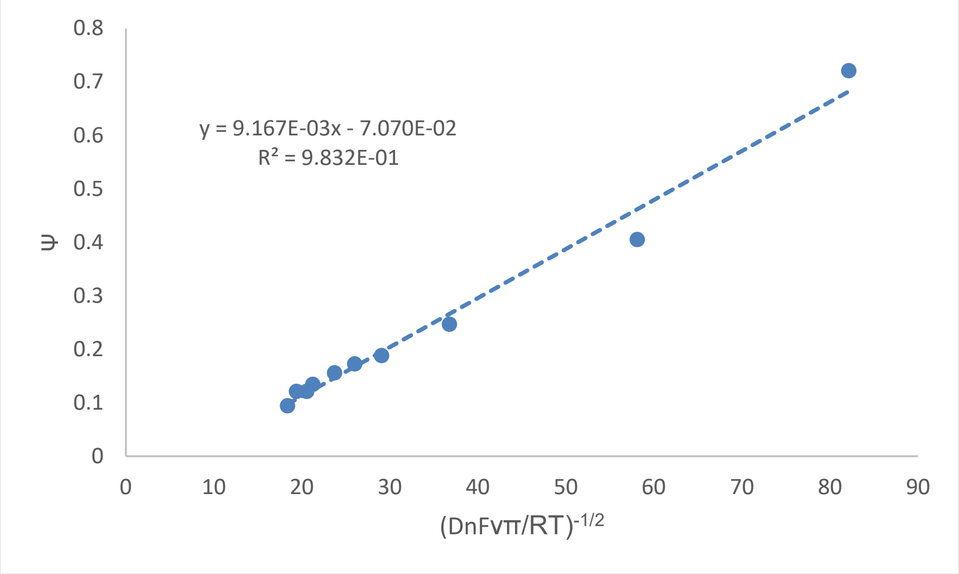

Figure S5: Nicholson analysis of the $^{CF3}bpy^{0/\cdot-}$ couple of $PPN_2Ru(^{CF3}bpy)(CN\text{-}BCF)_4$, with a slope of k_0.

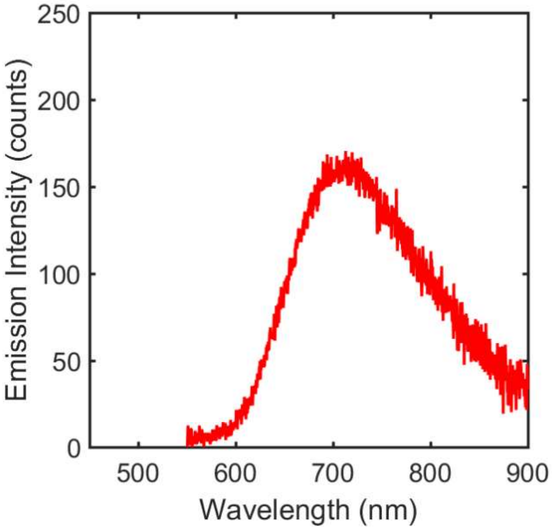

Figure S6: Steady-state emission spectrum of aqueous $K_2Ru(^{CF3}bpy)(CN)_4$ excited at 400 nm.

Table S1: Measurement of quantum yield for $PPN_2Ru(^{CF3}bpy)(CN\text{-}BCF)_4$.

Sample	A_{450}	*I*	φ_{ref}	φ_{sample} *wrt*
Aerated $[Ru(bpy)_3]^{2+}$ *1*	0.0747	8.30 x10^5	0.018	0.132
Deaerated $[Ru(bpy)_3]^{2+}$ *1*	0.1043	5.08 x10^6	0.095	0.159
Sample 1	0.0467	3.79 x10^6	-	-
Aerated $[Ru(bpy)_3]^{2+}$ *2*	0.0743	1.10 x10^6	0.018	0.131
Deaerated $[Ru(bpy)_3]^{2+}$ *2*	0.0961	6.43 x10^6	0.095	0.153
Sample 2	0.0464	5.00 x10^6	-	-
				0.144 average

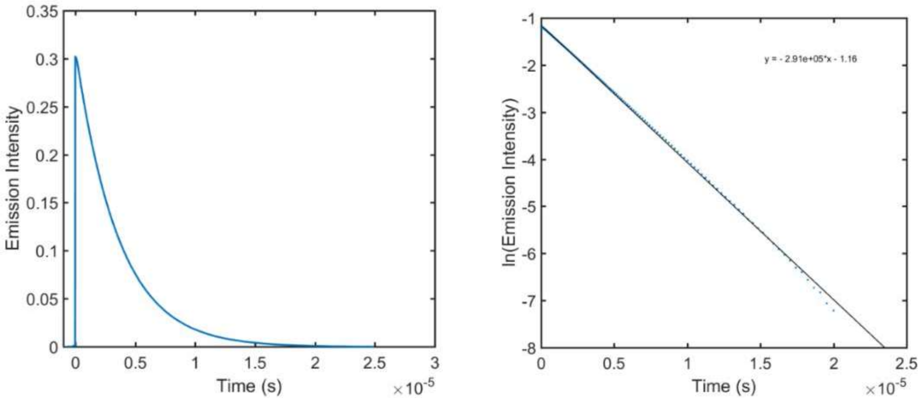

Figure S7: Left, time-resolved luminescence data for $PPN_2Ru(^{CF3}bpy)(CN\text{-}BCF)_4$. Right, linear fit to determine lifetime. The slope of the fit is the inverse of $\tau = 3.44$ μs.

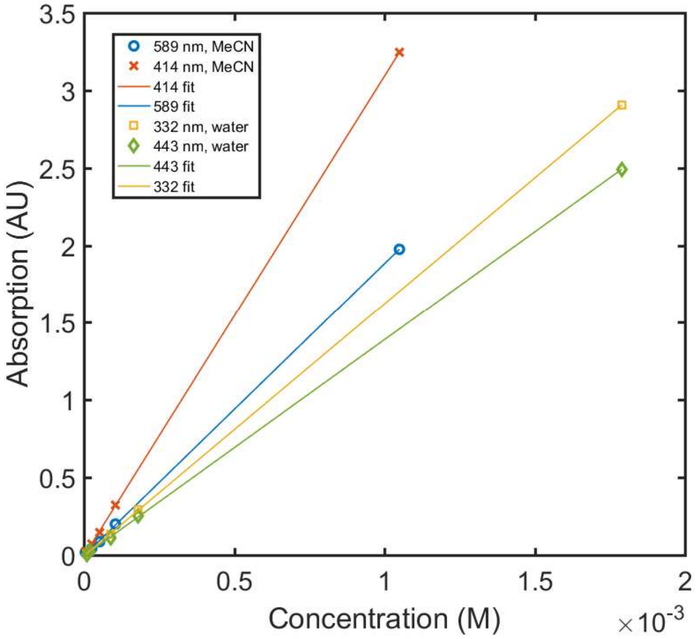

Figure S8: Dilution series for molar absorptivity of $[Ru(^{CF3}bpy)(CN)_4]^{2-}$ (K salt in water, PPN salt in MeCN) and linear fits. All measurements in 5 mm cuvette. Extinction coefficients are ε_{332} = 3660 $M^{-1}cm^{-1}$, ε_{443} = 3170 $M^{-1}cm^{-1}$ in water and ε_{414} = 6190 $M^{-1}cm^{-1}$, ε_{589} = 3770 $M^{-1}cm^{-1}$ in MeCN.

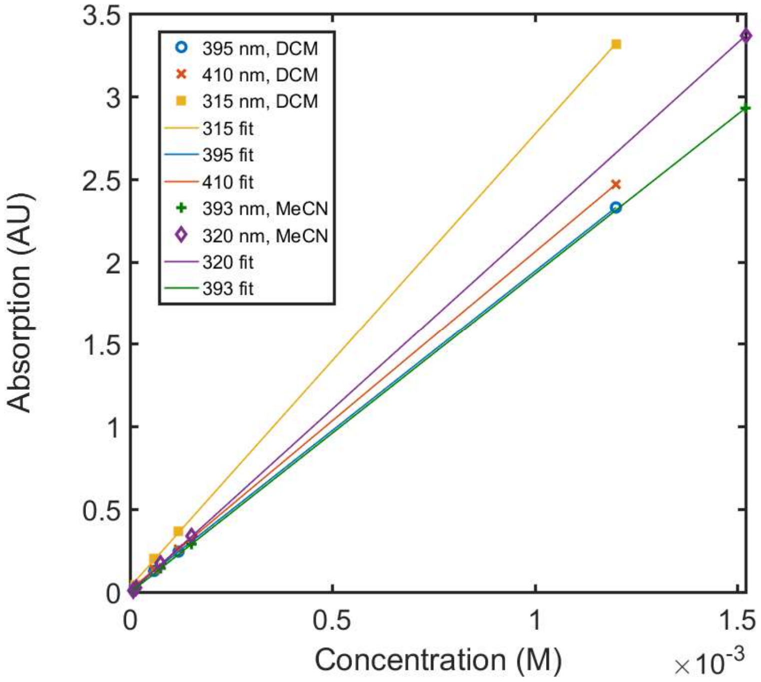

Figure S9: Dilution series for molar absorptivity of $PPN_2Ru(^{CF3}bpy)(CN\text{-}BCF)_4$ and linear fits. All measurements in 5 mm cuvette. Extinction coefficients are $\varepsilon_{315} = 1460\ M^{-1}cm^{-1}$, $\varepsilon_{395} = 958\ M^{-1}cm^{-1}$, $\varepsilon_{410} = 1020\ M^{-1}cm^{-1}$ in DCM and $\varepsilon_{320} = 3860\ M^{-1}cm^{-1}$, $\varepsilon_{393} = 4440\ M^{-1}cm^{-1}$ in MeCN.

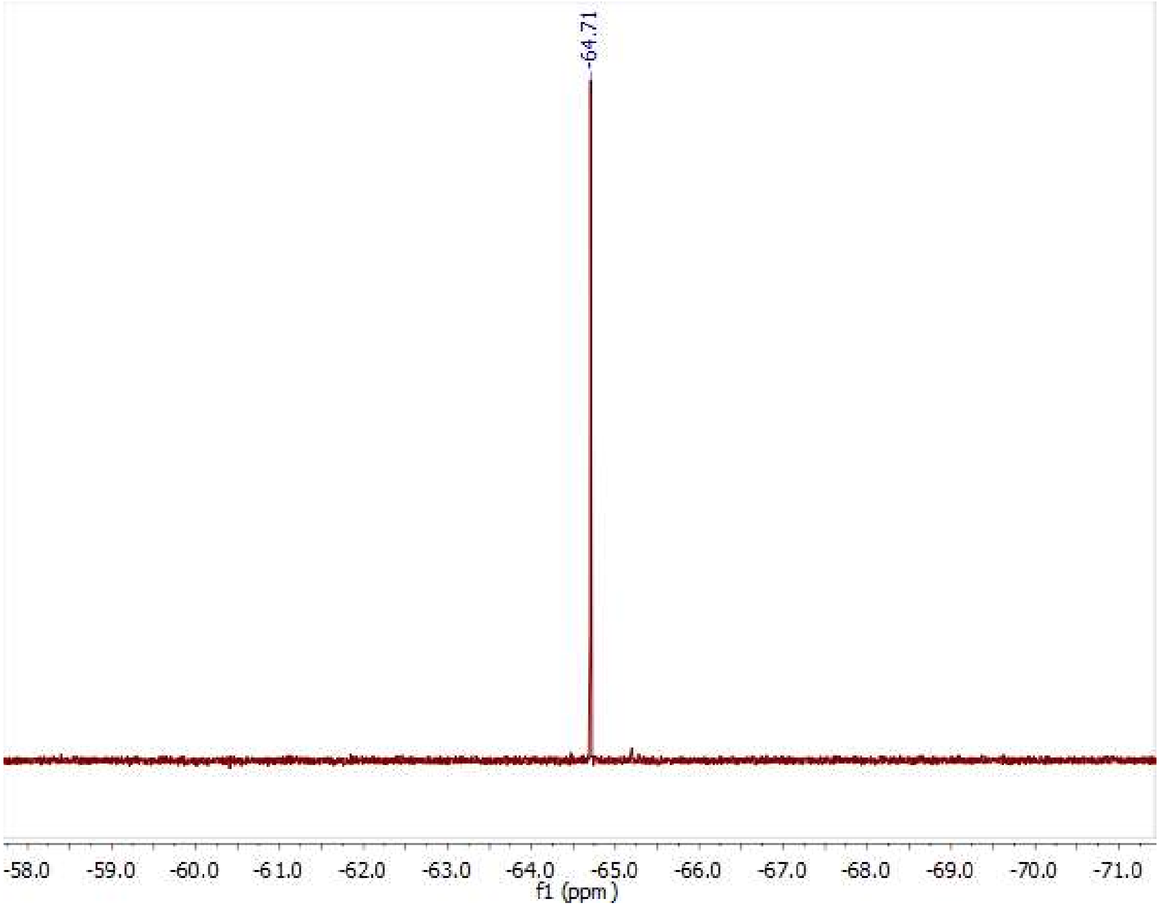

Figure S10: ^{19}F NMR spectrum of $PPN_2Ru(^{CF3}bpy)(CN)_4$ in CD_2Cl_2.

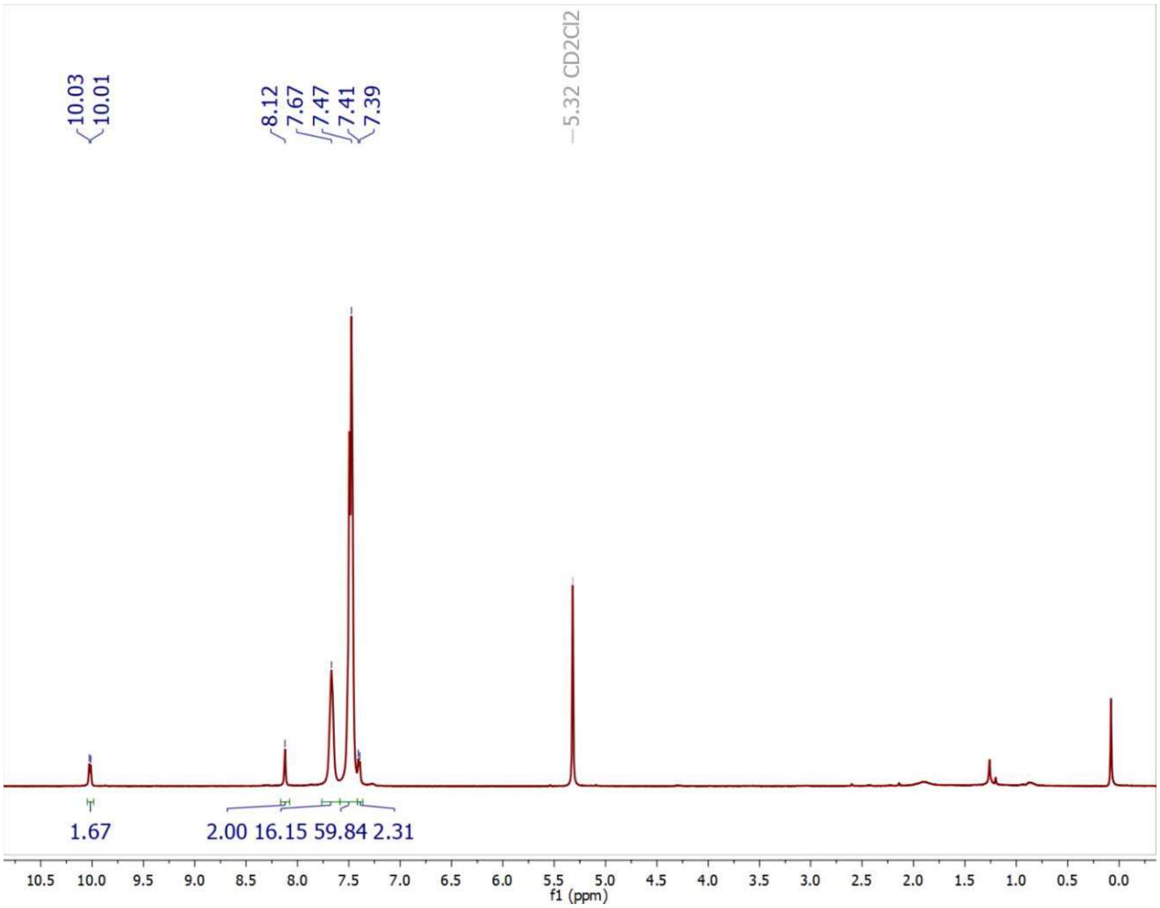

Figure S11: ^{1}H NMR spectrum of $PPN_2Ru(^{CF3}bpy)(CN)_4$ in CD_2Cl_2. Peaks upfield of 3 ppm are attributable to water, trace solvents, and silicone grease.

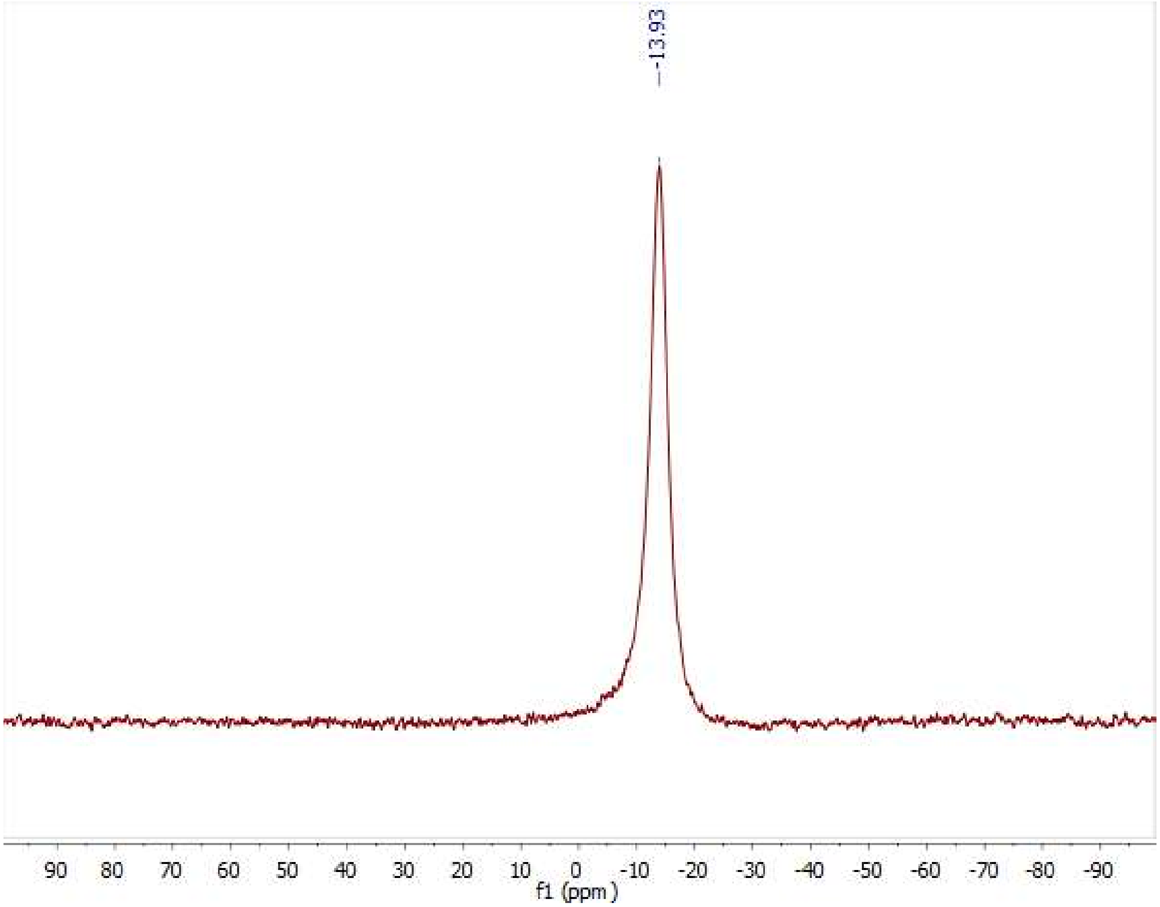

Figure S12: ^{11}B NMR spectrum of PPN$_2$Ru(^{CF3}bpy)(CN-BCF)$_4$ in CD$_2$Cl$_2$ acquired in a quartz NMR tube.

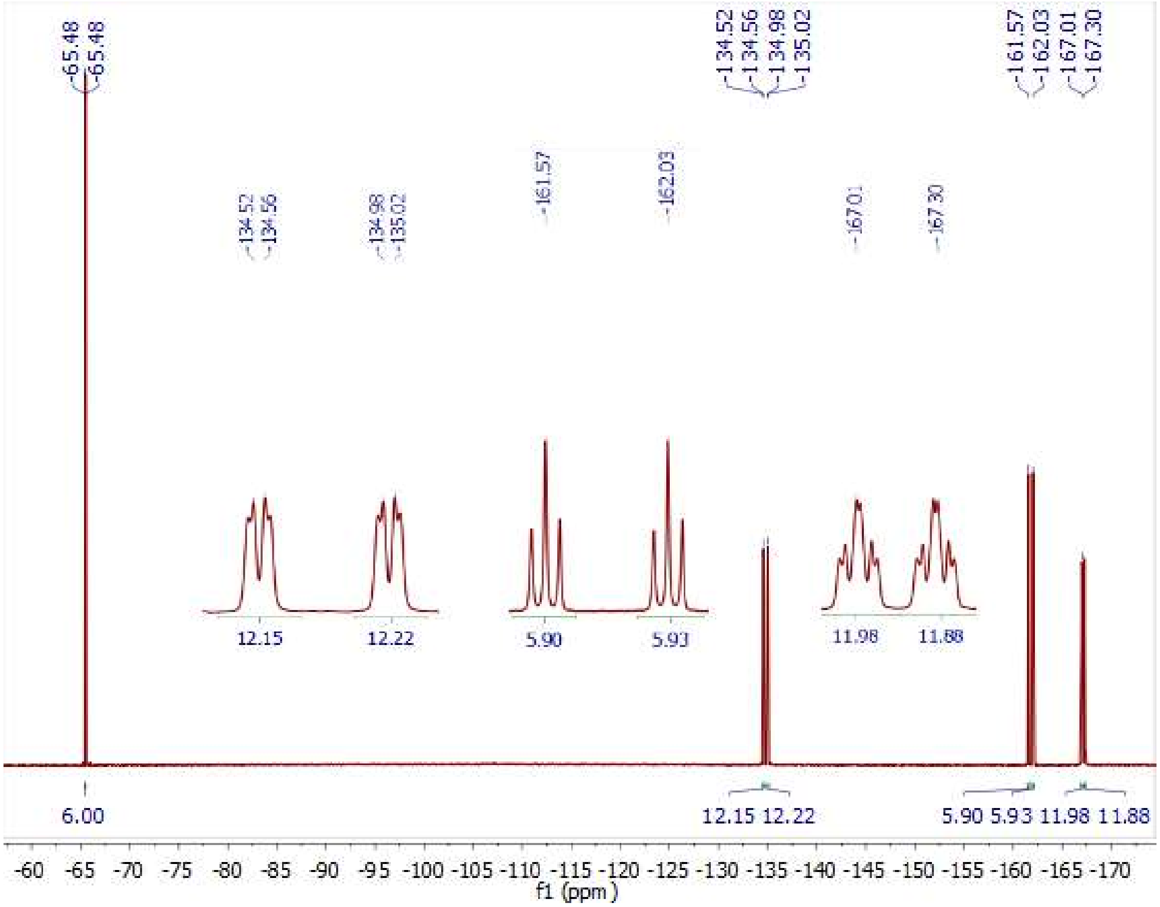

Figure S13: ^{19}F NMR spectrum of PPN$_2$Ru(^{CF3}bpy)(CN-BCF)$_4$ in CD$_2$Cl$_2$ with insets showing detail of BCF peaks.

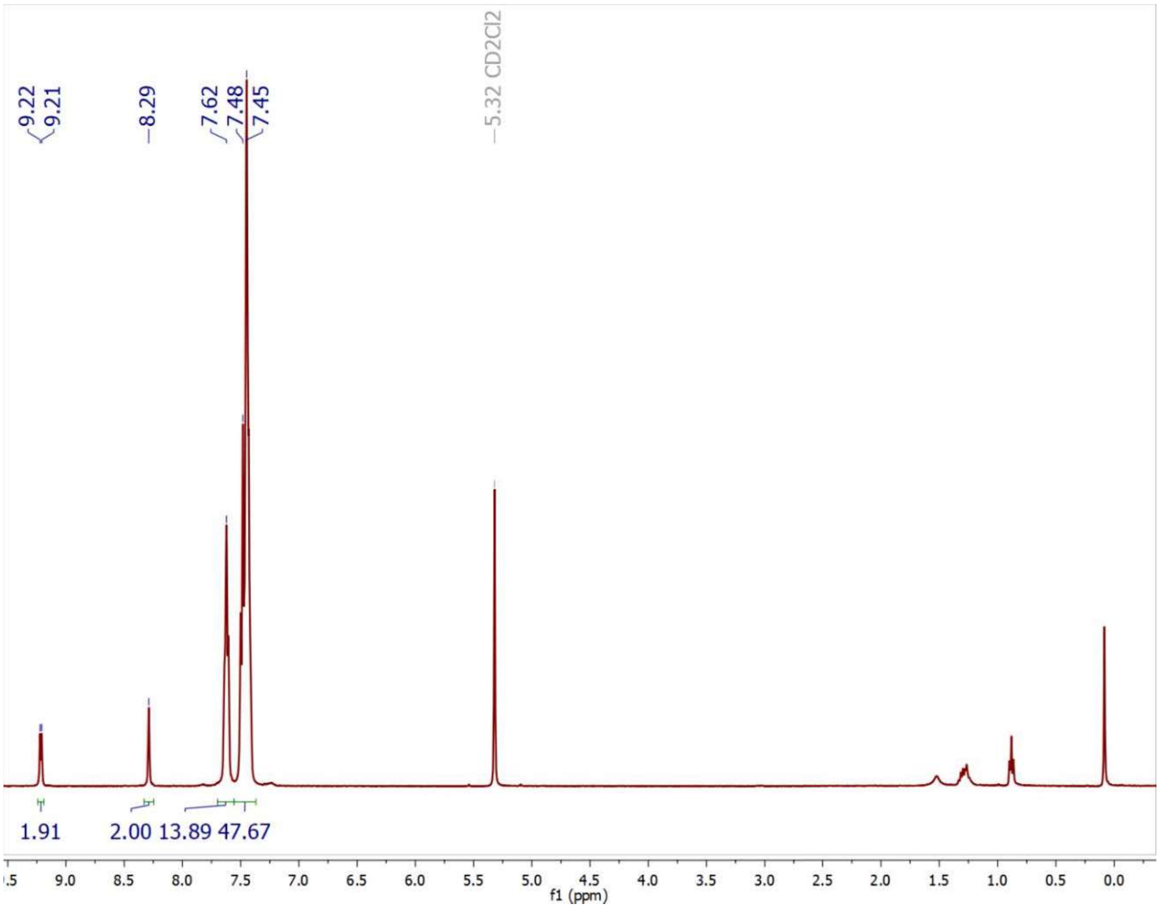

Figure S14: ^{1}H NMR spectrum of PPN$_2$Ru(^{CF3}bpy)(CN-BCF)$_4$ in CD$_2$Cl$_2$. Peaks upfield of 2 ppm are attributable to water, pentane, and silicone grease.